



Soft X-ray Radiation and Monte Carlo Simulations: Good Tools to Describe the Radiation Chemistry of Sub-keV Electrons

Lucie Huart, Christophe Nicolas, Josiane Kaddissy, Jean-Michel Guigner,
Alain Touati, Marie-Françoise Politis, Pascal Mercère, Benoît Gervais,
Jean-Philippe Renault, Marie-Anne Hervé Du Penhoat

► To cite this version:

Lucie Huart, Christophe Nicolas, Josiane Kaddissy, Jean-Michel Guigner, Alain Touati, et al.. Soft X-ray Radiation and Monte Carlo Simulations: Good Tools to Describe the Radiation Chemistry of Sub-keV Electrons. *Journal of Physical Chemistry A*, In press, 124 (10), pp.1896-1902. 10.1021/acs.jpca.9b10539 . cea-02496226

HAL Id: cea-02496226

<https://cea.hal.science/cea-02496226>

Submitted on 3 Mar 2020

HAL is a multi-disciplinary open access archive for the deposit and dissemination of scientific research documents, whether they are published or not. The documents may come from teaching and research institutions in France or abroad, or from public or private research centers.

L'archive ouverte pluridisciplinaire **HAL**, est destinée au dépôt et à la diffusion de documents scientifiques de niveau recherche, publiés ou non, émanant des établissements d'enseignement et de recherche français ou étrangers, des laboratoires publics ou privés.

Soft X-Ray Radiation and Monte Carlo Simulations: Good Tools to Describe the Radiation Chemistry of Sub-keV Electrons

Lucie Huart,^{†,‡,¶} Christophe Nicolas,[‡] Josiane A. Kaddissy,^{¶,⊥} Jean-Michel Guigner,[†] Alain Touati,[†] Marie-Françoise Politis,[§] Pascal Mercere,[‡] Benoit Gervais,^{||} Jean-Philippe Renault,[¶] and Marie-Anne Hervé du Penhoat^{*,†}

[†]*IMPMC, Sorbonne Université, UMR CNRS 7590, MNHN, Paris, France.*

[‡]*Synchrotron SOLEIL, Saint Aubin, France.*

[¶]*NIMBE, UMR CEA-CNRS 3685, Saclay, France.*

[§]*LAMBE UMR 8587, Université d'Evry val d'Essonne, CNRS, CEA, Université Paris-Saclay, 91025, Evry, France.*

^{||}*CIMAP, UMR 6252, Caen, France.*

[⊥]*Current address: Orano, Tour Areva, 1 Pl. Jean-Millier, 92400, Courbevoie, Paris La Défense, France.*

E-mail: marie-anne.herve_du_penhoat@upmc.fr

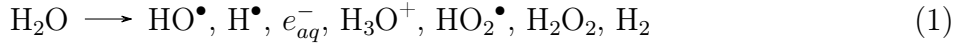
Phone: +33 (0)1 44 27 72 05

Abstract

The description of the biological effects of ionizing radiation requires a good knowledge of the dose deposition processes at both the cellular and molecular scales. However, experimental studies on the energy deposition specificity of sub-keV electrons, produced by most radiations, including high-energy photons and heavy ions, are scarce. Soft X-rays (0.2 - 2 keV) are here used to probe the physical and physico-chemical events occurring upon exposure of liquid water to sub-keV electrons. Liquid water samples were irradiated with a monochromatic photon beam at the SOLEIL synchrotron. Hydroxyl radical quantification was conducted through HO[•] scavenging by benzoate to form fluorescent hydroxybenzoate. Yields of HO[•] radicals exhibit a minimum around 1.5 keV, in good agreement with indirect observation. Moreover, they are relatively independent of the benzoate concentration in the range investigated, which corresponds to scavenging times of 170 ns to 170 ps. These results provide evidence that sub-keV electrons behave as high linear energy transfer particles, since they are able to deposit tens to hundreds of electronvolts in nanometric volumes.

Introduction

The radiation chemistry of liquid water has been extensively studied for the past sixty years in the context of radiotherapy, radioprotection and the nuclear industry. The radiation energy is deposited through ionization and excitation of the molecules in the medium by both the primary particle and all the secondary electrons generated along its path. These molecules thus subsequently undergo a dissociation process, leading to the formation of various radical and molecular products (eq 1).



Primary yields, defined as the yield of radicals and molecules formed after approximately one microsecond, are closely related to the spatial structure of the track, defined by the

ensemble of ionizations and excitations generated along the path of the primary particle and secondary electrons. As the linear energy transfer (LET) of the projectiles increases, the yield of radical species decreases while that of molecular products increases. This is due to enhanced sub-microsecond intra-track reactions when the density of ionizations and excitations increases. For instance, the HO[•] primary yield was shown to decrease from 2.8 to 1.0 HO[•]/100 eV, as the LET of protons increased from 0.3 to 20 keV/ μ m.¹

Although water radiolysis has been much investigated, there is an obvious lack of experimental studies on the properties of electrons in the sub-keV energy range. This scarcity is easy to understand owing to the very short tracks, a few nanometers, of these electrons in condensed matter. However, a precise description of the energy deposition processes in this energy range is required to understand the nanodosimetry of Auger emitters,² the radiosensitization by nanoparticles³ and the formation of complex DNA damage in high energy electrons track ends.⁴ We emphasize this latter point, as many indications point to a critical role of such complex lesions in the lethality induced by ionizing radiations.⁴ In such schemes, track-end electrons may act like high LET particles, as they deposit their whole energy in nanometric volumes. The efficiency of low energy electrons at inducing clusters of ionizations at the nanometer scale, and thus unrepairable complex DNA damage, has been underlined in several studies.⁵

The spatial structure of the tracks of keV and sub-keV electrons in liquid water has been studied by Monte Carlo (MC) simulations.^{6,7} As pointed out by the authors,⁷ the performance of such codes, especially at low energies, critically depends on the reliability of the interaction cross sections that are used as input in the simulation. Although elastic and inelastic diffusion cross sections are well established when the target water molecules are in gas phase,⁸ very few studies give those cross sections in the liquid phase. For inelastic scattering, condensed-phase effects can be accounted for through the complex dielectric response function of the liquid water.⁹ More recently, double differential cross sections for liquid water ionization upon 250 and 500 eV electron impact have been calculated by means of a com-

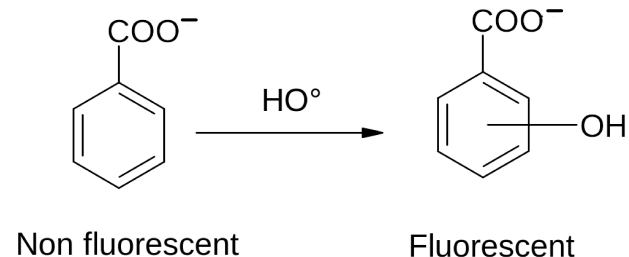
pletely *ab initio* model.^{10,11} In this model, a realistic description of the wavefunction for an isolated water molecule in the liquid phase is achieved by means of a Wannier orbital formalism. These calculations show that despite a similar qualitative behaviour for the liquid^{10,11} and vapour¹² phases, results present significative differences for the outermost orbitals. Total cross sections, which are mandatory input for Monte Carlo codes, have however not yet been established in this framework. Nevertheless, these total cross sections have been calculated for electron impact energy from 20 eV to 10 keV¹³ with a unified methodology to express the molecular wavefunctions of water in both vapor and liquid phases by means of a single-center approach. The authors conclude that the influence of the water phase on the ionization process are all the more important that the incident energy decreases and particularly critical in the sub-keV range.

To the best of our knowledge, direct measurement of liquid water radiolysis by low energy electrons (0.2 - 2 keV) is not reported in the literature, presumably because of their very low penetration depth in water (below 100 nm⁷). However, soft X-ray photons (0.2 - 2 keV) may be used to generate low energy electrons in water. Due to the very strong attenuation of such low energy X-rays (the attenuation length in water is below 20 μm ¹⁴), irradiation experiments in liquid water have mainly been performed for energies above 1.5 keV, measuring iron(II) sulphate (Fricke solution) oxidation yields.^{15,16} More recently, Fulford and coworkers have published the only experimental work in the sub-keV range. They determined the dependence of the primary yield of HO• radical (G_{OH}) on photon energy using aqueous solutions of plasmid DNA as a probe to sample the number of hydroxyl radicals present at the spur expansion completion (or homogenization) time, that is $\sim 10^{-6}$ s after the initial deposition of energy.¹⁷ These authors measured the yield of single-strand breaks (SSB) induced within the DNA probe when irradiated with photons varying in energy from 0.28 keV (C_K X-rays) to 1.25 MeV (^{60}Co γ -rays). The data, when normalized to the yield of SSB for ^{60}Co γ -rays, were then used as an estimate of G_{OH} (taking $G_{OH} \simeq 2.80$ molecule/100eV for ^{60}Co γ radiation at $\sim 10^{-6}$ s). The minimum in the HO• yield around 1.5 keV was attributed to a higher

ionization density leading to enhanced intra-track reactions. Several theoretical calculations for electrons^{18–20} or photons,²¹ using both analytical models and stochastic simulations, predicted the same general shape for G_{OH} versus particle energy curve, with a minimum HO• radical yield occurring between 0.1 and 1 keV, in partial agreement with Fulford *et al.*'s experimental data.

However, the data of Fulford *et al.* give no indication about the early time dependence of the radiolytic yields, which is a critical signature of the track structure²² and is crucial in concentrated biological media. A great part of the current knowledge concerning the early dynamics of ionization tracks following irradiation of water comes from studies involving the chemical scavenging method,²² which is based on measuring the concentration of the final stable products created in the irradiation of water and probe solutions. In this method, transient species, such as hydroxyl radicals, are converted into stable product by reaction with a probe molecule. The variation of the probe concentration allows a time reconstruction of the radical concentrations. However, the sensitivity of most scavenging methods are poor precluding their use with low intensity beams.

We have devised a new strategy combining the extraction of a soft X-ray synchrotron beam²³ and the use of a sensitive hydroxyl profluorescent probe.²⁴ This strategy allowed us to measure hydroxyl radical yields upon exposure to 200 to 1400 eV photons, as well as this yield at different scavenging times. We chose to focus on the yield of hydroxyl radicals not only because it is highly relevant for radiobiology but also because its yield is very sensitive to the ionization track density, i.e. the denser the ionization track, the less HO• radicals scavenged. Indeed, primary radiolytic species such as hydroxyl radicals, despite their short lifetimes (few μ s), can be quantified by reaction with scavengers to form stable products.²⁵



Scheme 1: Hydroxyl radical quantification scheme.

Methods

Radical Quantification Method

All chemicals used for this study are Sigma Aldrich products of the highest available purity, without any further purification, prepared using ultrapure Millipore Milli-Q water with a resistivity of $18.2 \text{ M}\Omega \cdot \text{cm}$ and less than 10 ppb organic carbon. Hydroxyl radical quantification was conducted through HO^\bullet scavenging by benzoate (Bz) to form fluorescent hydroxybenzoate (Scheme 1) in the presence of oxygen. Systematic calibrations of the fluorescence intensity were performed by adding a variable amount of 2-hydroxybenzoate ($10^{-7} - 10^{-3} \text{ M}$) to representative benzoate concentrations ($10^{-3} - 1 \text{ M}$). As a reference, the solutions were also irradiated with ^{137}Cs γ -rays at a 5 Gy/min dose rate (Gammacell, Best Theratronic).

Irradiation Setup and X-Ray Beam

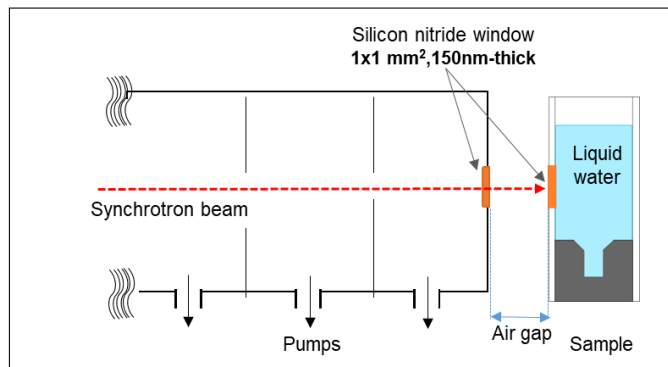


Figure 1: Experimental setup.

Irradiations were performed at the Metrologie beamline of the SOLEIL synchrotron (Saint Aubin, France). The experimental setup, initially developed for mammalian cells irradiation at the LURE synchrotron,^{26–28} has been adapted for the present study (Figure 1). Briefly, the setup is connected to the soft X-ray branch of the Metrologie beamline. To perform irradiation in air, the horizontal photon beam was extracted from the beamline through a three-stage differential vacuum system enclosed by a square $1 \times 1 \text{ mm}^2$ and 150 nm-thick silicon nitride window [in a square silicon frame \(\$10 \times 10 \text{ mm}^2\$ and 500 \$\mu\text{m}\$ thick\)](#) (FASTEC, Northampton, UK). The differential pumping system protects the Metrologie beamline and the synchrotron ring, in case of a failure of the 150 nm-thick silicon nitride window, due to mechanical stress.

The 1 ml water and probe solution is contained in a cell closed by another square $1 \times 1 \text{ mm}^2$ and 150 nm-thick silicon nitride membrane [in a square silicon frame \(\$10 \times 10 \text{ mm}^2\$ and 500 \$\mu\text{m}\$ thick\)](#), positioned 1 to 3 mm from the exit window. The beam size at the sample position is 0.3 mm wide, and the height varies between 0.5 and 1 mm depending on the opening of the exit slit of the monochromator. The cell is a PMMA semi micro cuvette, in which a 7 mm hole is drilled to allow the fixation of the silicon nitride membrane. The top surface of the solution is in contact with air during irradiation. All solutions initially contained the amount of O₂ that is naturally dissolved under normal conditions of pressure and temperature.

Dosimetry

The average dose absorbed in the solution was calculated using the following equation: $D = \frac{EN_0}{m}$, where E is the photon energy, N_0 is the number of photons at the solutions surface (i.e. immediately after the silicon nitride membrane) and m is the mass of the sample.

In the present work, average dose rates are lower than 0.2 Gy/min (Table 1). However, the attenuation length of the soft X-ray beams in water varies between 1 and 5 μm , leading to

much higher dose rates at the surface of the sample. Surface doses were estimated using the following equation : $D = \frac{EN_0}{S} \left(\frac{\mu}{\rho} \right)_{solution}$, where S is the area of the photon beam, estimated to be 0.3 mm^2 below 400 eV and 0.15 mm^2 at 1280 eV, and $(\mu/\rho)_{solution}$ is the mass absorption coefficient of the solution, calculated from elemental absorption coefficient.¹⁴

Table 1: Irradiation conditions

E (eV)	Average dose rate (Gy/min)	Attenuation length in water (μm) ¹⁴	Surface dose rate (kGy/min)
215	8.33×10^{-4}	0.95	2.9
350	2.49×10^{-3}	3.3	2.5
400	2.10×10^{-3}	4.7	1.5
1280	0.138	4.7	200

At 1280 eV, the high surface dose rates could lead to benzoate and molecular oxygen depletion in the surface layer of the sample. However, samples were irradiated one hour to achieve the smallest average doses (8.5 Gy), and these species thus undergo significant diffusion during irradiation. Using very unfavorable approximations, we show that the benzoate concentration would be reduced by approximately 20% at the surface of the 1 mM NaBz solution, and the O₂ concentration, by approximately 34% (see supporting information, sections 2 and 3). Note, however, that this estimate completely neglects the O₂ feeding through the air/water interface and the actual concentration is certainly less reduced. Moreover, we assumed that depletion of oxygen is due to its reaction with damaged Bz. This is a stringent hypothesis, as the production of reaction between Bz and HO[•], a Bz–OH adduct, has a significant lifetime that can allow it to diffuse out of the irradiation zone before reacting with O₂.²⁹ A 20% Bz depletion is not expected to significantly change BzOH yields.³⁰

In the 0.2 - 1.5 keV energy range, less than 1% of the photons are absorbed in benzoate when the sodium benzoate concentration is 0.01 mol/L. At a concentration of 1 mol/L, about 8% of the photons are absorbed in benzoate at 1280 eV, mainly in oxygen and carbon K-shells, and 5% in sodium, mainly its K-shell. Such events could damage benzoate molecules very efficiently and induce specific radiolysis processes. However, even assuming a 100% destruction efficiency upon photoabsorption in BzNa, only 0.01 molecule / 100 eV would be

destroyed by these events in the 1 mol/L solution. This yield is negligible with respect to the destruction yield of water molecules, which is the order of 5 to 6 molecules / 100 eV.

Beam Intensity Measurement.

Photon intensity was recorded before and after each irradiation with a photodiode (AXUV-100 G Ti/C from International Radiation Detector, Torrance, California, USA). It is coated with titanium and carbon films whose mean thicknesses are 190 ± 19 and 50 ± 5 nm, respectively, according to the constructor. This detector has a very stable quantum efficiency.³¹ Its response was nonetheless regularly compared to that of a second similar photodiode, to check for radiation damage. It was also regularly compared to that of a third in-line photodiode, and found to be similar within a few percent at 1280 eV, when the exit slit is less than about 0.3 mm. An additional photodiode (S3588-08 Si PIN photodiode from Hamamatsu Photonics K.K., Hamamatsu City, Japan) was inserted directly into the radiolysis cell to control the beam position at 1280 eV. Uncertainties related to beam alignment are thus considered negligible compared to the other sources of uncertainty.

Higher Order Photons.

The X-ray beam delivered by the diffraction grating contains unwanted high-order harmonics. Below 400 eV, second-order X-rays were partially eliminated by differential absorption in the air gap between the silicone nitride exit window and the surface of the sample. Moreover in-line 0.7 μm carbon and 0.5 μm titanium filters were used during 215 and 350 - 400 eV photon irradiation, respectively. The higher order photon contribution was measured from air attenuation measurements [at 1280 eV](#), and from absorption through in-line calibrated foils which selectively absorb first order photons, a 0.5 μm aluminum foil at 215 eV and a 0.7 μm carbon foil at 350 and 400 eV. Higher order contribution to the dose is estimated to be less than a few percent.

Monte Carlo Simulations

The MC simulation follows the work of several authors and our method is described in reference 32, where the radiolysis process is decomposed into three temporal stages. We consider a uniform homogeneous medium made of liquid water in which molecular oxygen and benzoate are solvated at a prescribed concentration. The primary particles investigated are either monoenergetic electrons (0.18 - 600 keV) or photons (0.8 - 20 keV). The method for modeling electrons transport through water is well described in our previous papers, we will thus underline in this section the specifics related to photon absorption. For photons in this energy range, the photoelectric effect dominates in water. The first stage is the physical stage associated to photon absorption by the medium leading to water molecule ionization by photoelectric effect and to further excitation and ionization associated to the ejected electron transport through the liquid. The photoelectric cross section for water molecule ionization increases sharply at the oxygen K-edge. For energy above this threshold, a significant amount of double ionization of the water molecule takes place due to Auger process. During the physical stage all the electrons liberated by ionization are tracked down to thermal energy at 300 K, i.e. a kinetic energy $E_{kin} = 39 \text{ meV}$. Note that we do not consider in our simulation the possible ionization of the benzoate anions (Bz^-). The ionization threshold of solvated Bz^- is of the order of 6.0 eV and is thus below the excitation threshold of water. Despite its low concentration, it can represent a particularly efficient interaction channel for subexcitation electrons, which will lead to a partial destruction of the Bz^- scavengers, with no formation of hydroxylated products, and the liberation of one additional solvated electron in the track ends. The second stage is the fast reorganization of the ionized and excited molecules, including proton transfer to their first neighbor, and the solvation of the liberated electrons. During this stage, the doubly-ionized molecules create two hydronium ions and one oxygen atom rather than hydroxyl radical as observed for single ionization. At the end of the physico-chemical stage, we obtain a three-dimensional map of the species resulting from photon absorption by the liquid. Finally, the third stage consists

in the diffusion and reaction of all the generated species.^{32,33} It is simulated by means of a Kinetic Monte Carlo algorithm.³² During this stage we take into account the presence of the solvated species by means of the method suggested by Green.^{34,35} We consider thus a concentration of oxygen $C_{O_2} = 0.26$ mM associated to air pressure of 1 bar. The presence of O₂ has an important scavenging effect on solvated electron, which, in turn, protects the HO• from reaction with the electron. The benzoate concentration was varied between 1 and 10³ mM. We consider only its reaction with HO• by means of a diffusion controlled reaction, with a reaction rate 5.9×10^9 M⁻¹· s⁻¹.³⁶ We did not take into account the possible reaction of benzoate with solvated electrons as it is not expected to interfere with the hydroxylation of benzoate (see supporting information, section 4).

In the present simulation, we consider that the current of incident photons is sufficiently small so that the cumulated absorption does not lead to any significant track overlap. Each photon impact is thus followed individually up to 10 μ s and the yield is obtained as the average over a large number of impacts.

Results and Discussion

Considering the low average dose rates achieved in soft X-ray irradiation (Table 1), most traditional scavenging technics can not be used. We have introduced in radiolysis the use of the non-toxic benzoic acid³⁰ as a sensitive scavenger of HO• radicals.²⁴ This sensitivity comes from the formation of fluorescent hydroxylated benzoates (HB, Scheme 1). The HO• concentration can be deduced from that of hydroxylated benzoate (also called salicylate) through a 30% hydroxylation efficiency.²⁴ It is known in coumarin hydroxylation that the scavenging efficiency may vary slightly with the LET of the particle.³⁷ However, these variations are limited (20% overestimation of the HO• yield at the most in Ref. 37). Furthermore, the relative evolution of the hydroxyl concentration in time can be reconstructed by varying the benzoate concentration. As the sodium benzoate is soluble at 1 mol/L and its scavenging

constant is $5.9 \times 10^9 \text{ M}^{-1} \cdot \text{s}^{-1}$, we have access to the hydroxyl yield on a 150 ps time scale.²⁴

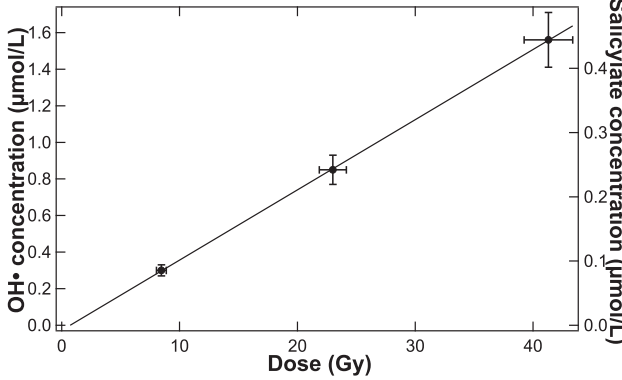


Figure 2: Concentration of HO^\bullet radicals formed in aerated 0.01 mol/L sodium benzoate solutions irradiated with 1280 eV X-rays (black symbols) as a function of dose. Statistical uncertainties only are shown. An additional systematic uncertainty of 4% must be taken into account.

Figure 2 shows the HO^\bullet concentration in 0.01 mol/L sodium benzoate solutions irradiated with 1280 eV X-rays as a function of dose. A linear increase is observed and the slope corresponds to the HO^\bullet yield. It is equal to $0.038 \pm 0.003 \mu\text{mol/J}$. This value is about two times smaller than that measured by Fulford and coworkers at 1487 eV (Al_K characteristic X-rays).¹⁷ However, our scavenging method is specific to HO^\bullet radicals, whereas Fulford et al. measure plasmid DNA single strand breaks, where additional direct effects cannot be excluded.

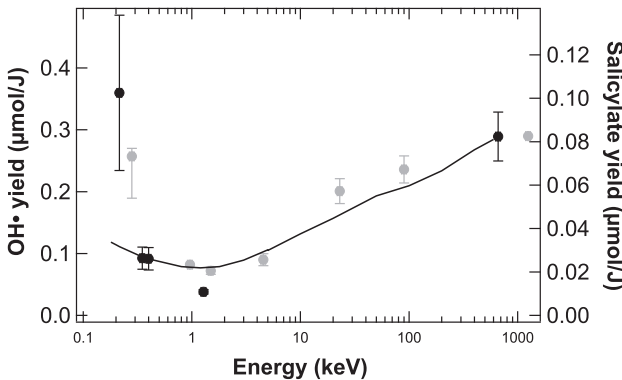


Figure 3: Yield of HO^\bullet radicals as a function of photons energy (black symbols). The benzoate sodium concentration is 0.01 mol/L. Measurements by Fulford et al.¹⁷ (grey symbols) are also presented. Experimental results are compared to Monte Carlo simulations for monoenergetic electrons (solid line).

Figure 3 shows the dependence of the HO[•] yield on photon energy. The overall shape in the present experiment is in good agreement with the data by Fulford et al.¹⁷ Our results obviously confirm the specificity of the 1 keV region where the HO[•] production is minimal. This minimum is attributed to an increase in the ionization density of the track that leads to strong intra-track recombination of HO[•] radicals. This is well reproduced by Monte Carlo simulations. The calculated HO[•] yield indeed exhibits a minimum around 1.2 keV when liquid water is irradiated with monoenergetic electrons (Figure 3, solid line). In the experiment, however, the sample is irradiated with soft X-rays, which predominantly interact with matter via the photoelectric effect. When the photons energy E is below that of the oxygen K-edge ($B_K = 0.54$ keV), photons are mainly absorbed in water outer shells. A single photo-electron is then emitted, and its energy is slightly lower than E . HO[•] yields are thus expected to be relatively similar for electrons and photons with the same energy E , at least when E is much larger than the outer shell electrons binding energy. Nonetheless, although a good agreement is observed between experiment and simulation around 400 eV, the simulation appears to underestimate the HO[•] yield at lower energies. As soon as photons have sufficient energy to remove oxygen K-shell electrons, this pathway is the most probable (~ 95%³⁸), leading to the emission of a photo-electron with energy $E - B_K$. The electronically excited system then relaxes *via* Auger decay within a few femtoseconds.³⁹ As a consequence an Auger electron is also emitted with ~ 0.5 keV energy. 1280 eV photons thus generate two spatially correlated electrons with ~ 500 and 700 eV. Our Monte Carlo simulation shows that the OH[•] yield of 0.4 - 1.2 keV individual electrons is ~ 0.08 - 0.09 $\mu\text{mol}/\text{J}$, very similar to that of 20 keV/ μm protons.¹ The measured HO[•] yield is however approximately two times lower. We have thus modeled the absorption of photons, either in outer or K shells of water. The calculation shows that HO[•] yields are 20% lower when 1280 eV photons are absorbed in oxygen K-shells than when they are absorbed in water outer shells. This differences decreases when the photon energy increases, as a larger fraction of its energy is transferred to the photo-electron which has a larger probability to interact with outer shells than with

inner shells (see supporting information, section 5).

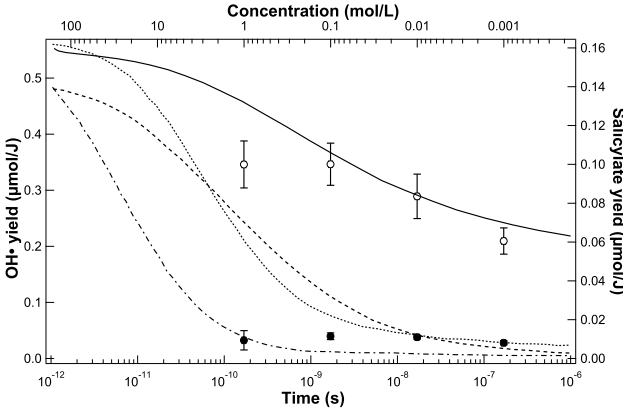


Figure 4: Yield of HO^\bullet radicals in aerated sodium benzoate solutions irradiated with 1280 eV X-rays (closed symbols) and ^{137}Cs γ -rays (open symbols), as a function of scavenging time. Experimental results are compared to results from Monte Carlo simulations³² for 2.6 keV/ μm protons (solid line) and 670 keV/ μm carbon ions (dashed line) and results from diffusion-kinetic models⁴⁰ for 100 (dotted line) and 1000 keV/ μm (dashed dotted line) particles.

Finally, we varied the Bz^- concentration in order to approach the initial hydroxyl production. Figure 4 shows the HO^\bullet yields in aerated sodium benzoate solutions irradiated with 1280 eV X-rays and ^{137}Cs γ -rays as a function of the scavenging time, from 170 ns to 170 ps (10^{-3} to 1 mol/L concentration range). Surprisingly, the HO^\bullet yield at 1280 eV appears relatively independent of the benzoate concentration. A possible limitation of the method, common to other scavenging methods,⁴¹ appears at high scavenger concentration. The initial stage of water radiolysis can indeed be affected by the presence of the scavenger, which can be significantly ionized by low energy electrons. One can also envision that increase in HO^\bullet scavenging with benzoate concentration leads also to an increase in reaction intermediates within the track and therefore, an increase in their probability of cross reaction. In such a case, the scavenging capacity is locally diminished and the HO^\bullet yield effectively measured is lower than the the actual yield. The significance of this effect is unfortunately rather difficult to estimate without a dedicated simulation. Keeping this in mind, we can still compare the gamma and 1.28 keV behaviors. In the scavenging time range investigated, the HO^\bullet production remains ten times lower than the production observed for gamma irradiation. This

behavior is characteristic of very high linear energy transfer radiations, such as heavy ions.⁴² The maximal LET expected for electrons is 25 - 30 eV/nm at ~ 200 eV.^{2,43-45} In this LET range, the expected hydroxyl yield should be higher than $0.1 \mu\text{mol}/\text{J}$ for scavenging times below the microsecond range.⁴⁶ Even taking into account the experimental uncertainties, our hydroxyl yield measurements are significantly lower. This high ionization density is confirmed by the time dependence of the HO[•] yield, which is presented in figure 4. By comparing to the data of Pimblott and LaVerne,⁴⁰ the time dependence suggest a LET close to or higher than 100 eV/nm. The question is then how to reconcile a LET lower than 30 eV/nm through physical simulation, and higher than 100 eV/nm through chemical effects for the same electrons. An obvious limitation of MC simulation is the uncertainty regarding the cross sections used to model the transport of low-energy electrons as discussed in recent papers.^{47,48} As mentioned previously, another possible explanation lies in the quasi-simultaneous production of two sub-keV electrons, the photo- and Auger electrons, that obviously may increase the local ionization density, compared to the emission of a single electron with the same total energy. The Monte Carlo simulation indeed shows a decrease in the HO[•] yields when the simultaneous emission of two electrons is taken into account. These yields are, however, still higher than the experimental results suggesting that the physico-chemical description underlying energy deposition initiated by K-shell ionizations should be precised. For instance, a possible destruction of the scavenger induced by K-shell ionization of its hydration layer was not taken into account. In cells, such events would lead to the formation of locally multiply damaged sites.²³

Conclusions

We have shown that combining a high sensitivity scavenging probe with a setup specifically designed to extract a soft X-ray beam in air, allowed us to quantify the hydroxyl yield formed upon irradiation of liquid water. This yield exhibits a minimum at ~ 1 keV, in agreement

with previous value deduced from indirect observation based on plasmid damage. Both the value and the time dependence of the HO[•] yield point to a very high linear energy transfer value for such photons. This is presumably the result of the high ionization density of the two electrons emitted after photoabsorption. This combined effect has been rarely evidenced and the biological impact of Auger emitters may be higher than previously thought. It would be interesting to use this strategy to investigate species, such as superoxide radicals,^{32,49} resulting from double ionization events and also to look at damage induced to biomolecules.

Acknowledgement

Soft X-rays experiments were carried out with the approval of Synchrotron SOLEIL (proposals numbers 99140122 and 20150164). The authors thank Paulo Dasilva for his help in connecting the experimental setup to the Metrologie beamline, and his support during the runs. The authors thank the SOLEIL biology and chemistry laboratories for their helpful support, as well as the Disco beamline for the use of their UV spectrometer. This Work was supported by ANR project HighEneCh (ANR-17-CE30-0017) and the NanoTheRad strategic Research Initiatives from Paris Saclay University.

Supporting Information Available

The following files are available free of charge.

- SI.pdf : Discussion about the high dose rate at the surface of the solution (track overlap, benzoate or O₂ depletion) **and about the reaction of hydrated electrons with benzoate. Comparison between the energy deposition following the absorption of a photon of energy E either in the outer shell or the K shell of water molecules.**

References

- (1) Frongillo, Y.; Goulet, T.; Fraser, M.-J.; Cobut, V.; Patau, J.-P.; Jay-Gerin, J.-P. Monte Carlo simulation of fast electron and proton tracks in liquid water-II. Nonhomogeneous chemistry. *Radiation Physics and Chemistry* **1998**, *51*, 245 – 254.
- (2) Kassis, A. I. The amazing world of Auger electrons. *International Journal of Radiation Biology* **2004**, *80*, 789–803, PMID: 15764386.
- (3) McMahon, S. J.; Hyland, W. B.; Muir, M. F.; Coulter, J. A.; Jain, S.; Butterworth, K. T.; Schettino, G.; Dickson, G. R.; Hounsell, A. R.; O'Sullivan, J. M. et al. Biological consequences of nanoscale energy deposition near irradiated heavy atom nanoparticles. *Scientific Reports* **2011**, *1*, 18.
- (4) Goodhead, D. T. Energy deposition stochastics and track structure: What about the target? *Radiation Protection Dosimetry* **2007**, *122*, 3–15.
- (5) Nikjoo, H.; Goodhead, D. T. Track structure analysis illustrating the prominent role of low-energy electrons in radiobiological effects of low-LET radiations. *Physics in Medicine and Biology* **1991**, *36*, 229–238.
- (6) Date, H.; Sutherland, K.; Hasegawa, H.; Shimozuma, M. Ionization and excitation collision processes of electrons in liquid water. *Nuclear Instruments and Methods in Physics Research Section B: Beam Interactions with Materials and Atoms* **2007**, *265*, 515 – 520.
- (7) Emfietzoglou, D.; Papamichael, G.; Nikjoo, H. Monte Carlo electron track structure calculations in liquid water using a new model dielectric response function. *Radiation Research* **2017**, *188*, 355–368, PMID: 28650774.
- (8) Itikawa, Y.; Mason, N. Cross sections for electron collisions with water molecules. *Journal of Physical and Chemical Reference Data* **2005**, *34*, 1–22.

- (9) Emfietzoglou, D.; Cucinotta, F. A.; Nikjoo, H. A complete dielectric response model for liquid water: A solution of the Bethe ridge problem. *Radiation Research* **2005**, *164*, 202–211.
- (10) de Sanctis, M. L.; Politis, M.-F.; Vuilleumier, R.; Stia, C. R.; Fojón, O. A. Theoretical study of the ionization of liquid water from its several initial orbitals by fast electron impact. *Journal of Physics B: Atomic, Molecular and Optical Physics* **2015**, *48*, 155201.
- (11) de Sanctis, M. L.; Politis, M.-F.; Vuilleumier, R.; Stia, C. R.; Fojón, O. A. Double differential cross sections for liquid water ionization by fast electron impact. *Eur. Phys. J. D* **2017**, *71*, 125.
- (12) Champion, C.; Hanssen, J.; Hervieux, P. A. Erratum: Influence of molecular orientation on the multiple differential cross sections for the $(e, 2e)$ process on a water molecule [Phys. Rev. A 63, 052720 (2001)]. *Phys. Rev. A* **2005**, *72*, 059906.
- (13) Champion, C. Electron impact ionization of liquid and gaseous water: A single-center partial-wave approach. *Physics in Medicine and Biology* **2009**, *55*, 11–32.
- (14) Henke, B.; Gullikson, E.; Davis, J. X-Ray interactions: photoabsorption, scattering, transmission, and reflection at $E = 50\text{--}30,000$ eV, $Z = 1\text{--}92$. *Atomic Data and Nuclear Data Tables* **1993**, *54*, 181 – 342.
- (15) Freyer, J. P.; Schillaci, M. E.; Raju, M. R. Measurement of the G-value for 1.5 keV X-rays. *International Journal of Radiation Biology* **1989**, *56*, 885 – 892.
- (16) Watanabe, R.; Usami, N.; Kobayashi, K. Oxidation yield of the ferrous ion in a Fricke solution irradiated with monochromatic synchrotron soft X-rays in the 1.8–10 keV region. *International Journal of Radiation Biology* **1995**, *68*, 113 – 120.
- (17) Fulford, J.; Bonner, P.; Goodhead, D. T.; Hill, M. A.; O'Neill, P. Experimental determination of the dependence of OH radical yield on photon energy: A comparison

- with theoretical simulations. *The Journal of Physical Chemistry A* **1999**, *103*, 11345 – 11349.
- (18) Magee, J. L.; A. Chatterjee, A. Theory of the chemical effects of high-energy electrons. *The Journal of Physical Chemistry* **1978**, *82*, 2219 – 2226.
- (19) Hill, M.; Smith, F. Calculation of initial and primary yields in the radiolysis of water. *Radiation Physics and Chemistry* **1994**, *43*, 265 – 280.
- (20) Pimblott, S. M.; LaVerne, J. A. Effect of electron energy on the radiation chemistry of liquid water. *Radiation Research* **1998**, *150*, 159–169.
- (21) Yamaguchi, H. A spur diffusion model applied to estimate yields of species in water irradiated by monoenergetic photons of 50 eV-2 MeV. *International Journal of Radiation Applications and Instrumentation. Part C. Radiation Physics and Chemistry* **1989**, *34*, 801 – 807.
- (22) Pimblott, S. M.; LaVerne, J. A.; Bartels, D. M.; Jonah, C. D. Reconciliation of transient absorption and chemically scavenged yields of the hydrated electron in radiolysis. *The Journal of Physical Chemistry* **1996**, *100*, 9412–9415.
- (23) Hervé du Penhoat, M.-A.; Eschenbrenner, A.; Abel, F.; Boissière, A.; Guigner, J.-M.; Chetioui, A.; Politis, M.-F.; Touati, A.; Sage, E.; Jenner, T. J. et al. Double-strand break induction and repair in V79-4 hamster cells: The role of core ionisations, as probed by ultrasoft X-rays. *International Journal of Radiation Biology* **2010**, *86*, 205 – 219.
- (24) Musat, R.; Moreau, S.; Poidevin, F.; Mathon, M. H.; Pommeret, S.; Renault, J. P. Radiolysis of water in nanoporous gold. *Phys. Chem. Chem. Phys.* **2010**, *12*, 12868–12874.

- (25) LaVerne, J. A.; Pimblott, S. M. Scavenger and time dependences of radicals and molecular products in the electron radiolysis of water: Examination of experiments and models. *The Journal of Physical Chemistry* **1991**, *95*, 3196–3206.
- (26) Hervé du Penhoat, M.-A.; Fayard, B.; Abel, F.; Touati, A.; Gobert, F.; Despiney-Bailly, I.; Ricoul, M.; Sabatier, L.; Stevens, D. L.; Hill, M. A. et al. Lethal effect of carbon K-shell photoionizations in Chinese hamster V79 cell nuclei: Experimental method and theoretical analysis. *Radiation Research* **1999**, *151*, 649–658.
- (27) Fayard, B.; Touati, A.; Abel, F.; Hervé du Penhoat, M.-A.; Despiney-Bailly, I.; Gobert, F.; Ricoul, M.; L'Hoïr, A.; Politis, M.-F.; Hill, M. A. et al. Cell inactivation and double-strand breaks: The role of core ionizations, as probed by ultrasoft X rays. *Radiation Research* **2002**, *157*, 128–140.
- (28) Gobert, F.-N.; Lamoureux, M.; Hervé du Penhoat, M.-A.; Ricoul, M.; Boissière, A.; Touati, A.; Abel, F.; Politis, M.-F.; Fayard, B.; Guigner, J. et al. Chromosome aberrations and cell inactivation induced in mammalian cells by ultrasoft X-rays: Correlation with the core ionizations in DNA. *International Journal of Radiation Biology* **2004**, *80*, 135–145.
- (29) Wu, C.; De Visscher, A.; Gates, I. D. Reactions of hydroxyl radicals with benzoic acid and benzoate. *RSC Adv.* **2017**, *7*, 35776–35785.
- (30) Armstrong, W. A.; Black, B. A.; Grant, D. W. The radiolysis of aqueous calcium benzoate and benzoic acid solutions. *The Journal of Physical Chemistry* **1960**, *64*, 1415–1419.
- (31) Korde, R.; Cable, J. S.; Canfield, L. R. One gigarad passivating nitrided oxides for 100% internal quantum efficiency silicon photodiodes. *IEEE Transactions on Nuclear Science* **1993**, *40*, 1655–1659.

- (32) Gervais, B.; Beuve, M.; Olivera, G.; Galassi, M. Numerical simulation of multiple ionization and high LET effects in liquid water radiolysis. *Radiation Physics and Chemistry* **2006**, *75*, 493 – 513.
- (33) Gervais, B.; Beuve, M.; Olivera, G.; Galassi, M.; Rivarola, R. Production of HO₂ and O₂ by multiple ionization in water radiolysis by swift carbon ions. *Chemical Physics Letters* **2005**, *410*, 330 – 334.
- (34) Green, N. J. Reaction probability and diffusion-controlled rate constants for ionic reactions in solvents of high permittivity. *Chemical Physics Letters* **1984**, *107*, 485 – 488.
- (35) Colliaux, A.; Gervais, B.; Rodriguez-Lafrasse, C.; Beuve, M. O₂ and glutathione effects on water radiolysis: A simulation study. *Journal of Physics: Conference Series* **2011**, *261*, 012007.
- (36) Buxton, G. V.; Greenstock, C. L.; Helman, W. P.; Ross, A. B. Critical Review of rate constants for reactions of hydrated electrons, hydrogen atoms and hydroxyl radicals ($\bullet OH/\bullet O^-$) in Aqueous Solution. *Journal of Physical and Chemical Reference Data* **1988**, *17*, 513–886.
- (37) Maeyama, T.; Yamashita, S.; Baldacchino, G.; Taguchi, M.; Kimura, A.; Murakami, T.; Katsumura, Y. Production of a fluorescence probe in ion-beam radiolysis of aqueous coumarin-3-carboxylic acid solution-1: Beam quality and concentration dependences. *Radiation Physics and Chemistry* **2011**, *80*, 535 – 539.
- (38) Yeh, J.; Lindau, I. Atomic subshell photoionization cross sections and asymmetry parameters: $1 \leq Z \leq 103$. *Atomic Data and Nuclear Data Tables* **1985**, *32*, 1 – 155.
- (39) Sankari, R.; Ehara, M.; Nakatsuji, H.; Senba, Y.; Hosokawa, K.; Yoshida, H.; Fannis, A. D.; Tamenori, Y.; Aksela, S.; Ueda, K. vibrationally resolved O 1s photoelectron spectrum of water. *Chemical Physics Letters* **2003**, *380*, 647 – 653.

- (40) Pimblott, S. M.; LaVerne, J. A. Diffusion-kinetic theories for LET effects on the radiolysis of water. *The Journal of Physical Chemistry* **1994**, *98*, 6136–6143.
- (41) Baldacchino, G.; Vigneron, G.; Renault, J.; Caér, S. L.; Pin, S.; Mialocq, J.-C.; Balanzat, E.; Bouffard, S. Hydroxyl radical yields in the tracks of high energy $^{13}\text{C}^{6+}$ and $^{36}\text{Ar}^{18+}$ ions in liquid water. *Nuclear Instruments and Methods in Physics Research Section B: Beam Interactions with Materials and Atoms* **2006**, *245*, 288 – 291, Swift Heavy Ions in Matter.
- (42) Baldacchino, G.; Maeyama, T.; Yamashita, S.; Taguchi, M.; Kimura, A.; Katsumura, Y.; Murakami, T. Determination of the time-dependent OH-yield by using a fluorescent probe. Application to heavy ion irradiation. *Chemical Physics Letters* **2009**, *468*, 275 – 279.
- (43) Emfietzoglou, D.; Nikjoo, H. Accurate electron inelastic cross sections and stopping powers for liquid water over the 0.1-10 keV range based on an improved dielectric description of the Bethe surface. *Radiation Research* **2007**, *167*, 110 – 120.
- (44) Nguyen-Truong, H. T. Low-energy electron inelastic mean free paths for liquid water. *Journal of Physics: Condensed Matter* **2018**, *30*, 155101.
- (45) Incerti, S.; Kyriakou, I.; Bernal, M. A.; Bordage, M. C.; Francis, Z.; Guatelli, S.; Ivanchenko, V.; Karamitros, M.; Lampe, N.; Lee, S. B. et al. Geant4-DNA example applications for track structure simulations in liquid water: A report from the Geant4-DNA Project. *Medical Physics* **45**, e722–e739.
- (46) Schuemann, J.; McNamara, A. L.; Ramos-Méndez, J.; Perl, J.; Held, K. D.; Paganetti, H.; Incerti, S.; Faddegon, B. TOPAS-nBio: An extension to the TOPAS simulation toolkit for cellular and sub-cellular radiobiology. *Radiation Research* **2019**, *191*, 125–138, PMID: 30609382.

- (47) Nikjoo, H.; Emfietzoglou, D.; Liamsuwan, T.; Taleei, R.; Liljequist, D.; Uehara, S. Radiation track, DNA damage and response—a review. *Reports on Progress in Physics* **2016**, *79*, 116601.
- (48) Shin, W.-G.; Ramos-Mendez, J.; Faddegon, B.; Tran, H. N.; Villagrasa, C.; Perrot, Y.; Okada, S.; Karamitros, M.; Emfietzoglou, D.; Kyriakou, I. et al. Evaluation of the influence of physical and chemical parameters on water radiolysis simulations under MeV electron irradiation using Geant4-DNA. *Journal of Applied Physics* **2019**, *126*, 114301.
- (49) Gaigeot, M.-P.; Vuilleumier, R.; Stia, C.; Galassi, M. E.; Rivarola, R.; Gervais, B.; Politis, M.-F. A multi-scale ab initio theoretical study of the production of free radicals in swift ion tracks in liquid water. *Journal of Physics B: Atomic, Molecular and Optical Physics* **2007**, *40*, 1–12.

Graphical TOC Entry

